

Introduction

Various in-situ observations (*McComas et al. 2008*) have shown that the variations of the solar magnetic field over the 11-year sunspot cycle has an impact on the Sun's environment, especially on the wind velocity and density distribution (cf. **Fig. 1**). We are especially interested in the influence of equatorial asymmetry, as the Sun shows a delay of a year on average between the two hemispheres' reversals (*Temmer et al. 2006*); **Fig. 2** shows the wind latitudinal distribution over time (*Sokol et al. 2015*), and we can notice an equatorial asymmetry as well. This asymmetry can be linked to the interplay between the two dynamo families. **Fig. 3** shows the quadrupole to dipole energy ratio over several cycles: the quadrupole is weak at minimum of activity but becomes dominant at reversals, showing the importance of the two dynamo families (*DeRosa et al. 2012*).

Our goal is to understand the link between the dynamo generated field and the resulting wind distribution and asymmetry. For that, we reproduce the equatorial asymmetry for the magnetic field and the wind by coupling the dynamo families. We also aim at recovering the wind velocity distribution and global variations such as mass loss.

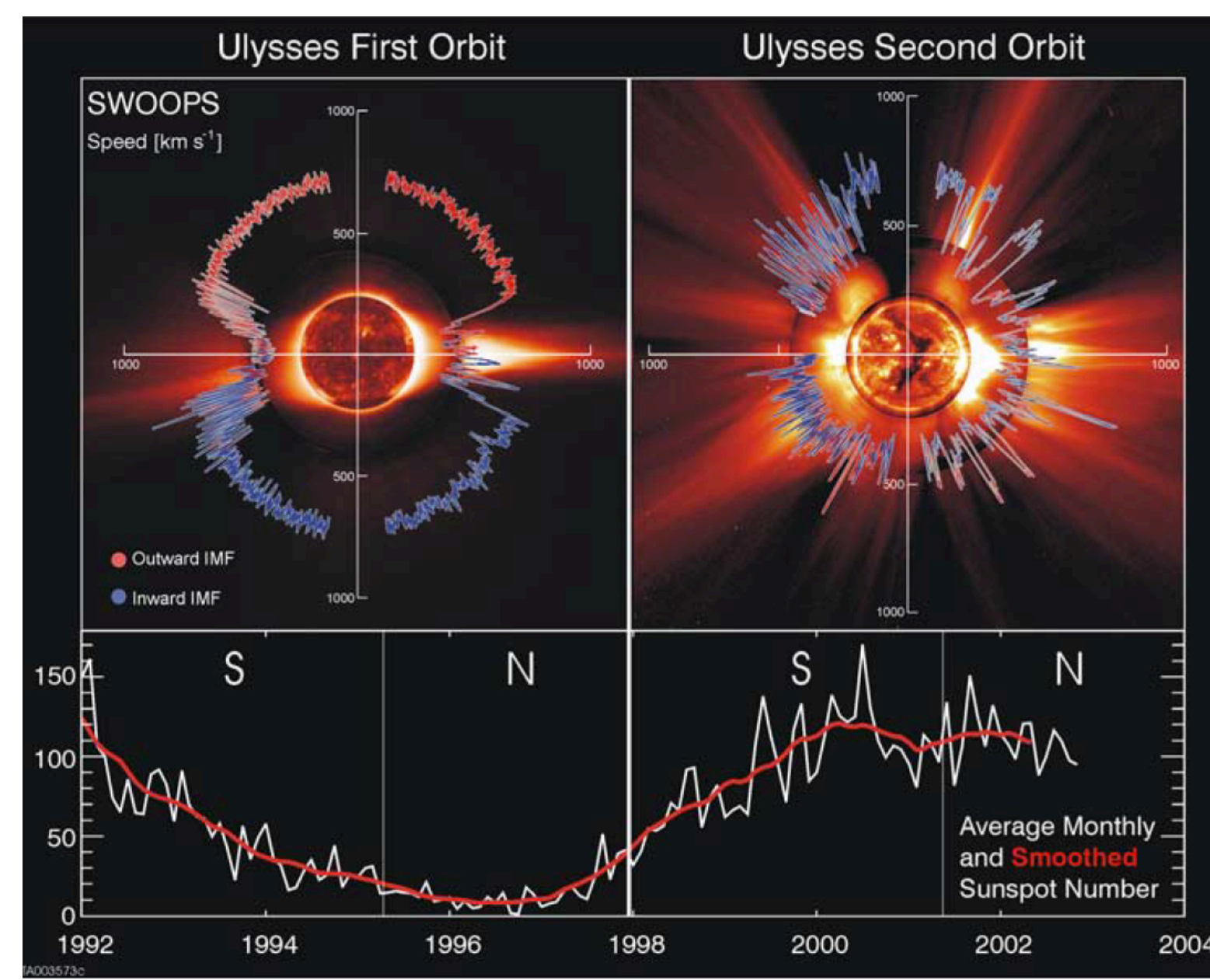
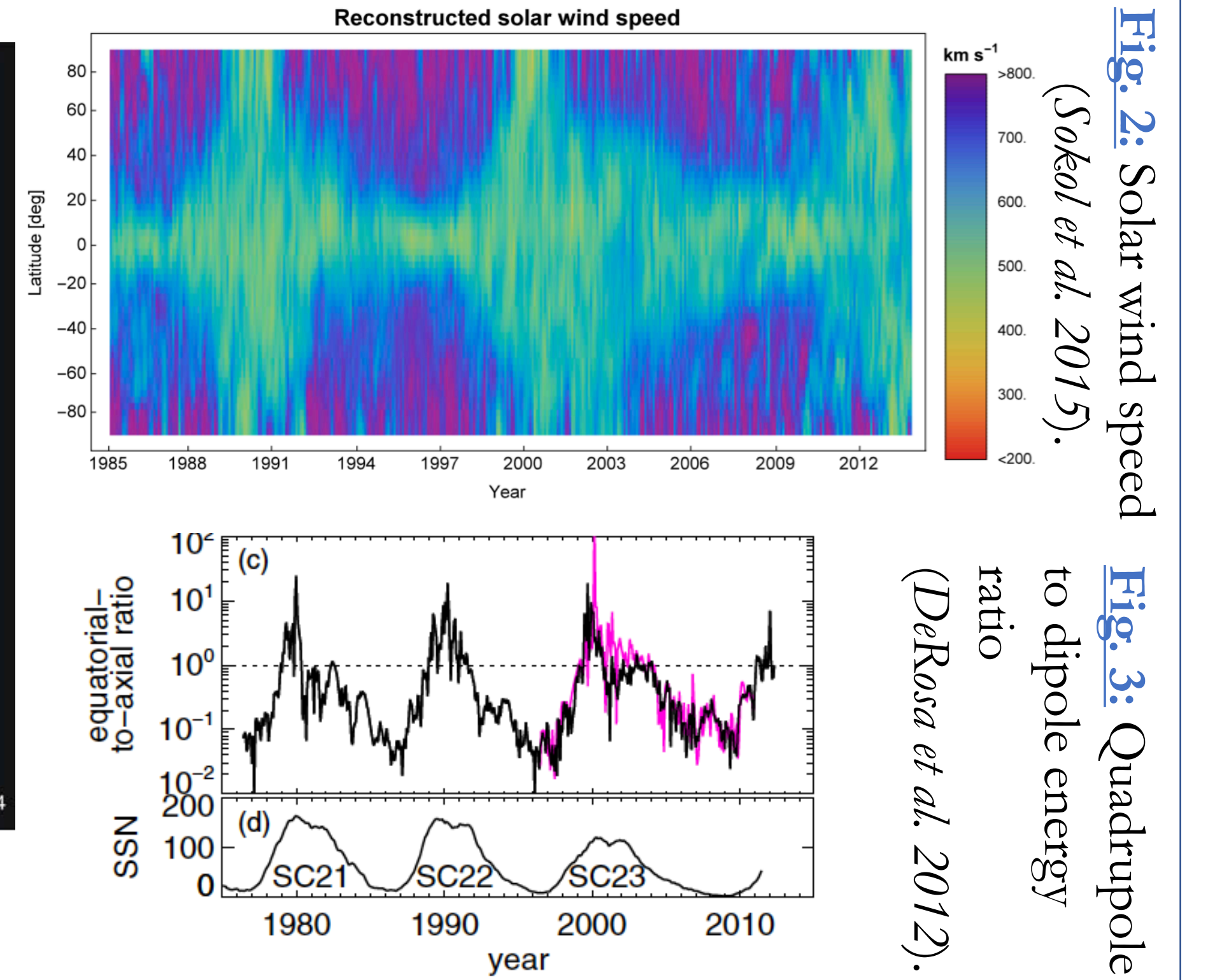


Fig. 1: Ulysses' results for wind speed and sunspot number (*McComas et al. 2008*).



Numerical set-up

We use 2 numerical codes to perform quasi-static simulations, following a study by *Pinto et al. (2011)*. The STELEM code (*Jouve & Brun 2007*) generates an asymmetric dynamo field through a 2.5D Babcock-Leighton mechanism over an entire cycle (cf. **Fig. 4**). We select 54 instants spaced by 2.5 months, and inject the corresponding magnetic field as a bottom boundary condition in the PLUTO code (*Mignone et al. 2007*) to perform 2.5D polytropic wind simulations (adapted from *Réville et al. 2015a*). We let the wind relax to reach a steady-state solution for each instant. In **Fig. 5** we can see the velocity projected on the magnetic field in units of Mach number (color) and the magnetic field lines (white lines), showing the distribution of streamers and their asymmetry during reversals (the streamers can be compared to **Fig. 1**).

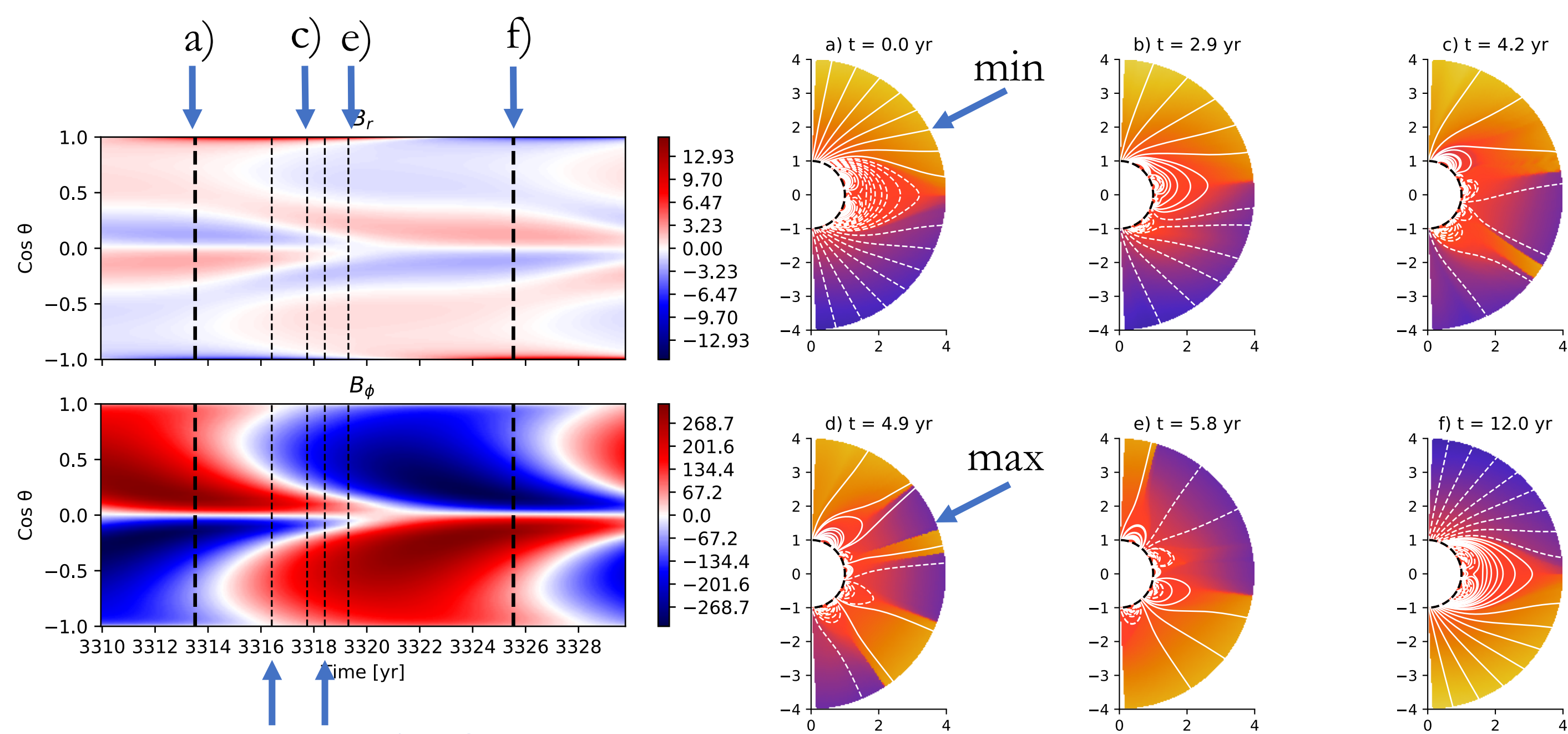


Fig. 4: Time-latitude diagrams for B_r and B_ϕ .

Fig. 5: $u \cdot B / (c_s ||B||)$ and magnetic field lines at different times.

Dynamo model field properties

Asymmetry:

Fig. 6 shows the time evolution of a proxy for the sunspot number in each hemisphere in our solar simulation. We see that there is a delay of 9 months between the two hemispheres maxima, with the southern hemisphere reversing first.

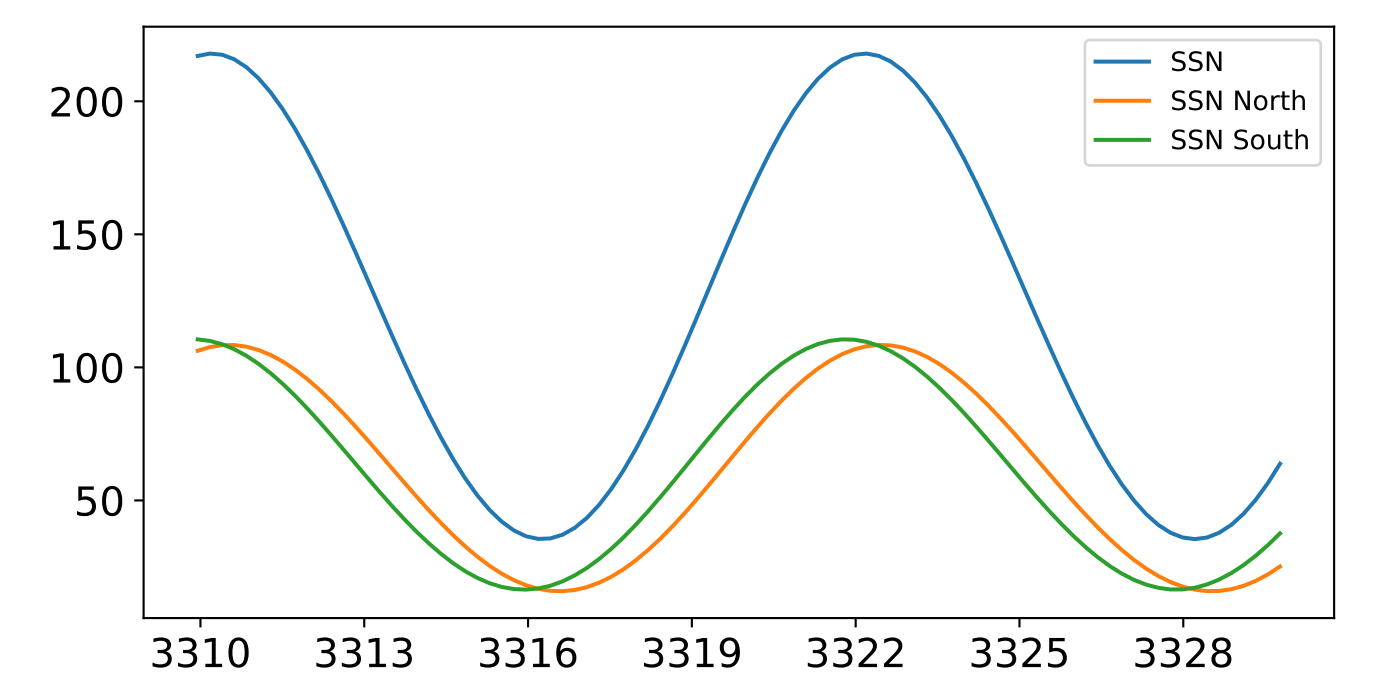


Fig. 6: Time evolution of proxy sunspot number in the two hemispheres.

Dynamo families in model:

Fig. 7 shows the time evolution of the primary (dipolar) and secondary (quadrupolar) dynamo families modes. We notice that the strongest mode is not the dipole, and that the quadrupole amplitude is about 10% of the dipolar family amplitude on average as a result of the asymmetry, thus more important than in most mean-field dynamo models.

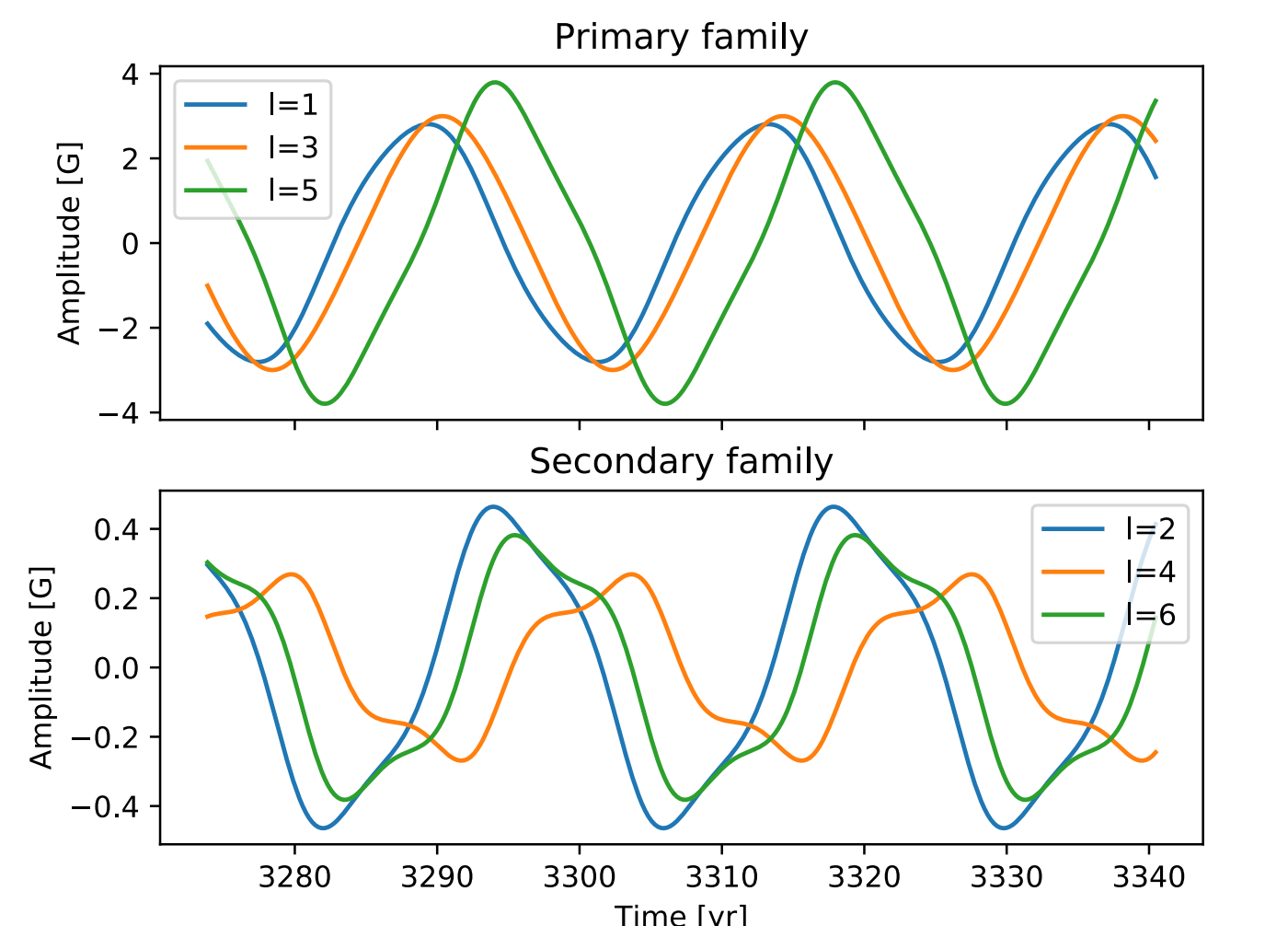


Fig. 7: Time evolution of the two dynamo families coefficients.

Results

Wind velocity:

Fig. 8 shows time evolution of the velocity latitudinal distribution of the wind over a cycle, from one minimum to the next, resulting from our 54 relaxed wind solutions. We recover the bimodal distribution at minimum (slow wind at the equator, fast wind at the poles) and slower wind everywhere at maximum. We obtain a delay between the slow-down at the poles in the two hemispheres as a consequence of the asymmetric dynamo. This is close to what has been observed in *Sokol et al. (2015)* in **Fig. 2** with the Interplanetary Scintillations (IPS) method.

NB: the wind velocity amplitude in **Fig. 8** is shown at $r = 20R_\odot$ in km/s; at $r = 215R_\odot = 1AU$, the range is between 450 and 530 km/s.

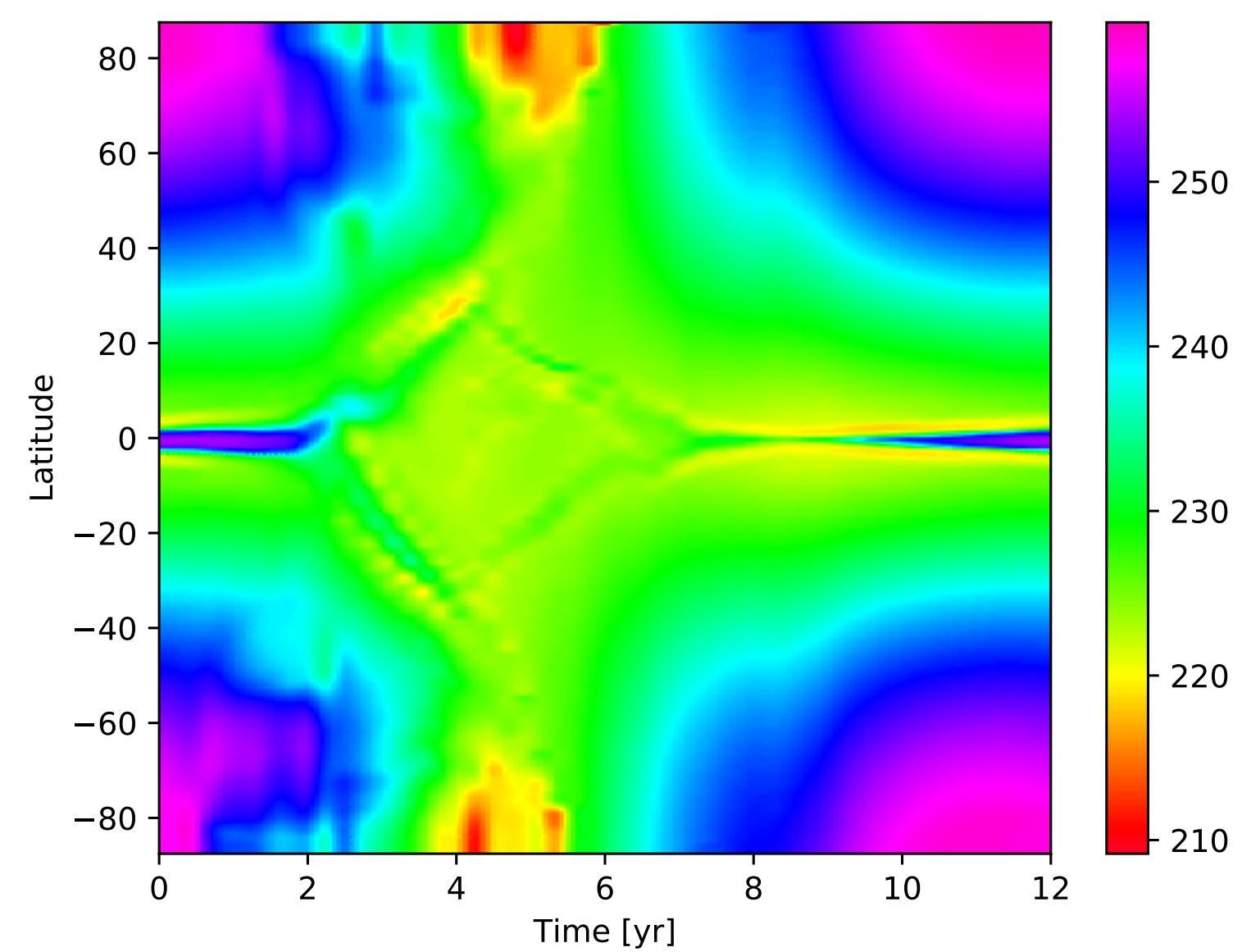


Fig. 8: Time-latitude diagram of wind speed.

Alfvén radius and mass flux:

Fig. 9 and 10 show the time evolution over a cycle of respectively the average Alfvén radius and the mass loss. We also show the time evolution of the parity factor (equal to -1 when the surface field is dipolar, 1 when quadrupolar) or the surface magnetic energy in black. The purple (yellow) lines indicate the beginning and end of reversal of the southern (northern) hemisphere.

In **Fig. 9**, the Alfvén radius is anti-correlated with the parity factor, which is expected. It varies between 2.5 and 5 solar radii, where estimations yields up to 12 solar radii; this is common with polytropic codes. It varies by a factor 2 over the cycle, which is a bit more than expected due to the axisymmetric assumption.

In **Fig. 10**, the mass loss varies between 2.67 and 2.87 $10^{-14} M_\odot/\text{yr}$, where estimations yields between 2.6 and 3.1 $10^{-14} M_\odot/\text{yr}$. In our model, since the dipole is not the strongest mode, the maximum of energy is not in phase with the reversal of the field, which allows us to clearly identify that the mass loss is more influenced by the total surface magnetic energy than the topology.

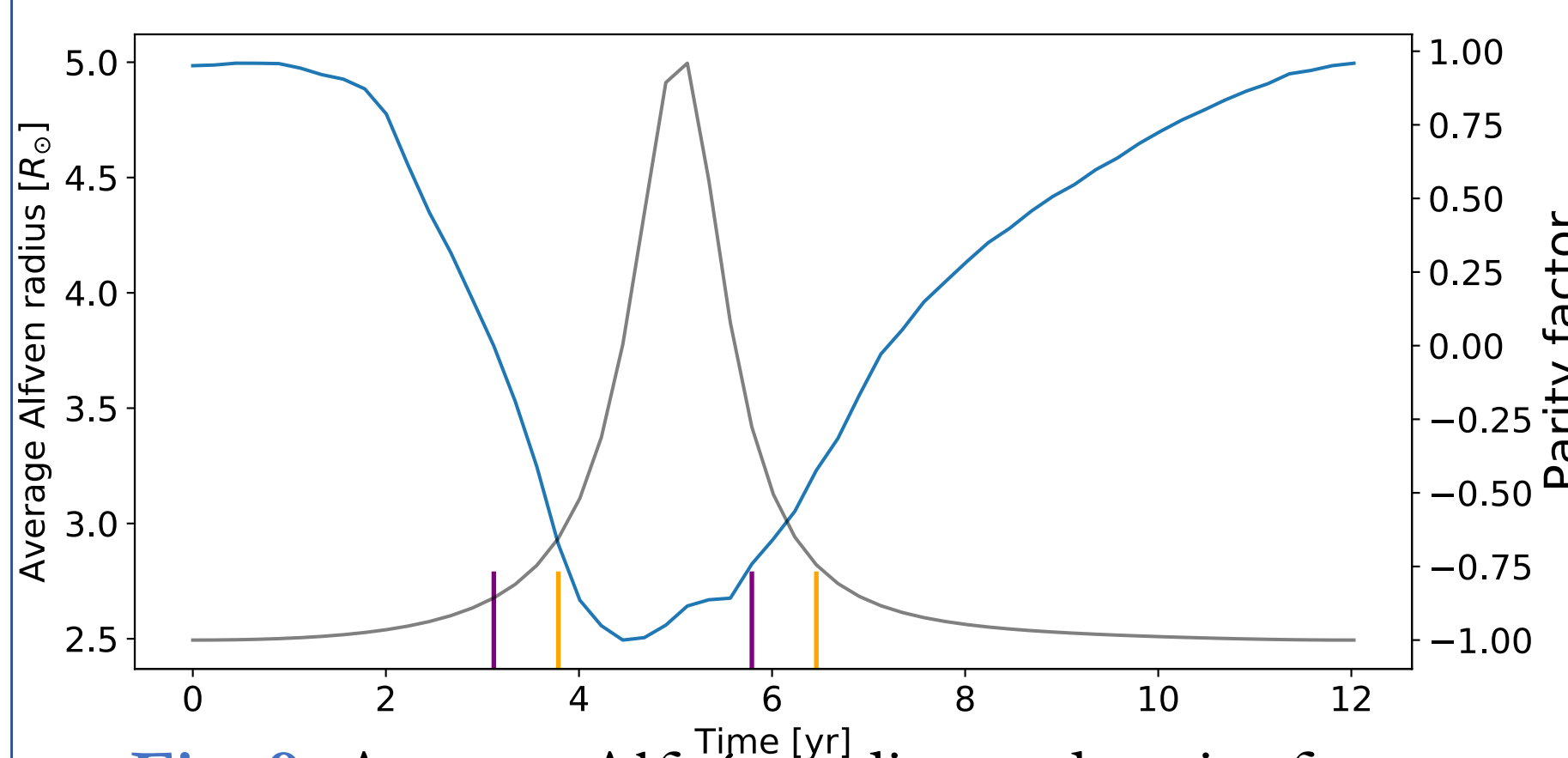


Fig. 9: Average Alfvén radius and parity factor evolution over a sunspot cycle.

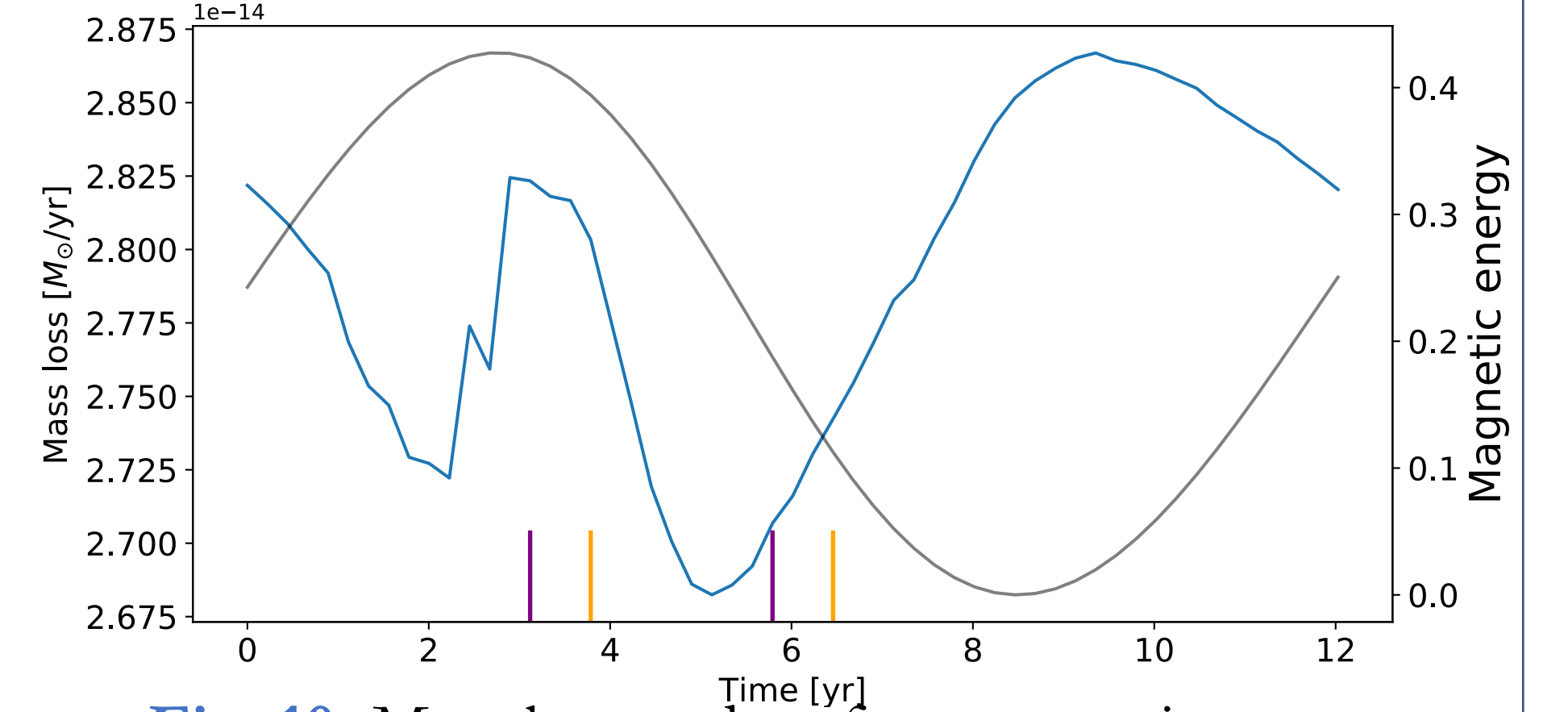


Fig. 10: Mass loss and surface magnetic energy evolution over a sunspot cycle.

Conclusion

- We have successfully recovered the dynamics of the corona over a sunspot cycle: at minimum of activity, we observe a large central streamer, resulting in slow wind at the equator and fast wind at the poles; at maximum, the multipolar topology of the field leads to slow and fast winds at all latitudes, with streamers emerging at mid-latitudes.
- The 9-month asymmetry introduced in the magnetic field is linked to the coupling of the dynamo families, and produces a 5-month asymmetry in the wind for the formation of streamers.
- We have shown that the Alfvén radius is more sensitive to topology, whereas the mass loss is more sensitive to the surface magnetic energy.
- Next steps will be to model a realistic heating of the corona and to introduce a dynamical coupling.

References

- DeRosa, M. L., Brun, A. S., & Hoeksema, J. T. 2012, *ApJ*, 757, 96
- Jouve, L., & Brun, A. S. 2007, *A&A*, 474, 239-250
- McComas, D. J., Ebert, R. W., Elliot, H. A., Goldstein, B. E., Gosling, J. T., Schwadron, N. A., & Skoug, R. M. 2008, *Geo. Res. Letters*, 35, L18103
- Mignone, A., Bodo, G., Massaglia, S., Matsakos, T., Tesileanu, O., Zanni, C., & Ferrari, A. 2007, *ApJ*, 170, 228-24
- Pinto, R. F., Brun, A. S., Jouve, L., & Grappin, R. 2011, *ApJ*, 737, 72
- Réville, V., Brun, A. S., Matt, S. P., Strugarek, A., & Pinto, R. F. 2015, *ApJ*, 798, 116
- Réville, V., & Brun, A. S. 2017, *ApJ*, 850, 45
- Sokol, J. M., Swaczyna, P., Bzowski, M., Tokumaru, M., *Solar Physics*, 290, 2589-2615
- Temmer, M., Rybák, J., Bendík, P., Veronig, A., Vogler, F., Otruba, W., Pötzi, W. & Hanslmeier, A. 2006, *A&A*, 447, 735-743